

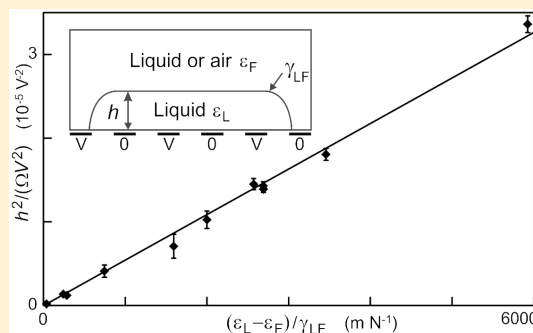
## Dielectrophoresis-Driven Spreading of Immersed Liquid Droplets

Carl V. Brown,<sup>\*,†</sup> Glen McHale,<sup>‡</sup> and Christophe L. Trabi<sup>†,‡</sup>

<sup>†</sup>Nottingham Trent University, School of Science & Technology, Clifton Lane, Nottingham NG11 8NS, United Kingdom

<sup>‡</sup>Northumbria University, Faculty of Engineering & Environment, Ellison Place, Newcastle upon Tyne NE1 8ST, United Kingdom

**ABSTRACT:** In recent years electrowetting-on-dielectric (EWOD) has become an effective tool to control partial wetting. EWOD uses the liquid–solid interface as part of a capacitive structure that allows capacitive and interfacial energies to adjust by changes in wetting when the liquid–solid interface is charged due to an applied voltage. An important aspect of EWOD has been its applications in microfluidics in chemistry and biology and in optical devices and displays in physics and engineering. Many of these rely on the use of a liquid droplet immersed in a second liquid due to the need either for neutral buoyancy to overcome gravity and shield against impact shocks or to encapsulate the droplet for other reasons, such as in microfluidic-based DNA analyses. Recently, it has been shown that nonwetting oleophobic surfaces can be forcibly wetted by nonconducting oils using nonuniform electric fields and an interface-localized form of liquid dielectrophoresis (dielectrowetting). Here we show that this effect can be used to create films of oil immersed in a second immiscible fluid of lower permittivity. We predict that the square of the thickness of the film should obey a simple law dependent on the square of the applied voltage and with strength dependent on the ratio of difference in permittivity to the liquid–liquid interfacial tension,  $\Delta\epsilon/\gamma_{LF}$ . This relationship is experimentally confirmed for 11 liquid–air and liquid–liquid combinations with  $\Delta\epsilon/\gamma_{LF}$  having a span of more than two orders of magnitude. We therefore provide fundamental understanding of dielectrowetting for liquid-in-liquid systems and also open up a new method to determine liquid–liquid interfacial tensions.



### INTRODUCTION

Controlling the wetting of liquids on surfaces can be achieved by modifying materials properties via surface chemistry modification<sup>1</sup> or the use of surfactants,<sup>2</sup> the use of surface texture to amplify surface chemistry induced tendencies, such as in superhydrophobicity,<sup>3,4</sup> or a combination of surface texture and liquid infusion, such as in slippery liquid-infused porous surfaces.<sup>5</sup> An alternative approach used in electrowetting, which provides active control, is to use an applied voltage to control the balance between the various interfacial energies and the capacitive energy resulting from the contact between a conducting droplet and an electrically insulating layer on a conducting contact.<sup>6,7</sup> This approach has proven effective in creating liquid lenses<sup>8</sup> and liquid paper<sup>9</sup> and in microfluidic systems.<sup>10,11</sup> A critical aspect has been to do so in liquid-in-liquid systems because of the need to remove the effects of gravity through neutral buoyancy, safeguard against impact shocks, or encapsulate a liquid that might otherwise evaporate.

A fundamental limitation of electrowetting is that although droplets can be made more wetting they cannot be induced into films irrespective of whether they are in air or immersed in a second liquid.<sup>12</sup> In contrast, liquid dielectrophoresis<sup>13</sup> can be used to induce partial wetting of droplets and to create dielectric liquid lenses.<sup>14–16</sup> Recently, we have elucidated the principles of dielectrowetting,<sup>17</sup> an interface-localized form of liquid dielectrophoresis that can be used to create films. It has been shown how it can be used to create voltage-programmable diffraction gratings<sup>18</sup> and optical shutters<sup>16,19,20</sup> or induce

voltage-controlled superspreading in air.<sup>21</sup> In considering how liquid dielectrophoresis can be viewed as an effect impacting on either the liquid–vapor interface or the solid–liquid and solid–vapor interfaces, the use of stripe experimental geometry based on coplanar interdigital electrodes has proved to be useful as it provides an electric field that decays exponentially with distance from the solid–liquid interface. This simplification allows the systems to be analytically modeled using minimization of surface free-energy approaches common to other problems in wetting and contact angles. However, our previous studies have been limited to liquid-in-air systems and have not experimentally addressed the important case of a liquid in a second immiscible liquid.

We develop a theoretical model of the dielectrowetting induced formation of films of one liquid immersed in a second immiscible fluid (air or liquid) that has a lower dielectric constant. We present experimental data for 11 different combinations of stripe-shaped droplets in fluids of lower dielectric constant with 6 of these being liquid–liquid combinations. Comparison of the model and data provides excellent agreement, suggesting that minimizing the surface free energy combined with the dielectrophoretic energy stored in the fluids is an effective physical description of the problem. Moreover, knowledge of the difference in permittivity between

**Received:** October 3, 2014

**Revised:** December 13, 2014

**Published:** December 17, 2014

the two liquids suggests this could be a new approach to enable liquid–liquid interfacial tensions to be measured. Alternatively, knowledge of the liquid–liquid interfacial tension between two liquids could allow the difference in permittivity to be determined.

## EXPERIMENTAL SECTION

Experiments were performed on liquid droplets resting on a borosilicate glass slide substrate while immersed in either air or in another immiscible liquid. A photograph and a schematic diagram of the experimental geometry are shown in Figure 1a,b, respectively. The

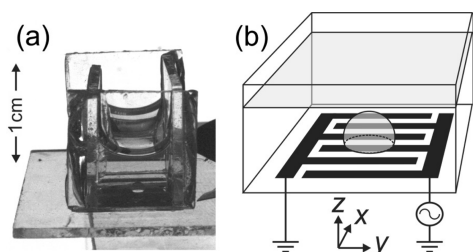


**Figure 1.** (a) Photograph of the device used in the experiments, with the scale indicated by the vertical arrow. (b) Schematic diagram of the experimental geometry: a liquid droplet rests on an array of interdigital electrodes while immersed in either air or in another immiscible liquid.

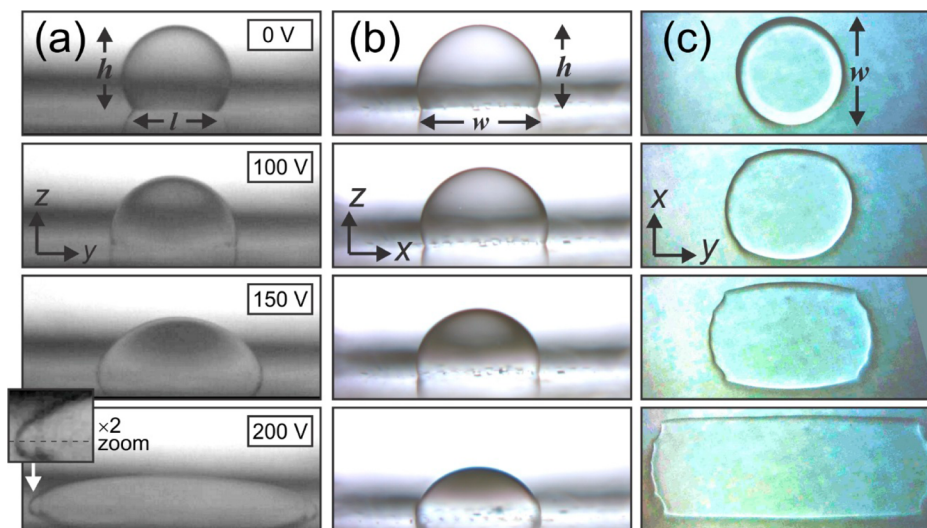
substrate was precoated with a 25 nm layer of indium tin oxide of resistivity 100 Ohm/square (Prazisions Glas and Optik, Iserlohn, Germany). On the substrate was an array of coplanar interdigital stripe electrodes for which both the electrode linewidths and the gaps between the electrodes were the same,  $d = 80 \mu\text{m}$ . The electrode pattern was produced using standard photolithographic procedures. The electrodes were coated with a  $0.7 \mu\text{m}$  capping layer of photoresist (SU8-10, MicroChem, Newton, MA) that was oxidized in a UV/ozone ProCleaner (Bioforce Nanoscience, Ames, IA) for 20 min. The substrate was finally treated with a commercial hydrophobic preparation (Granger's Extreme Wash-in, Grangers International, Alfreton, Derbyshire, U.K.) diluted to 1:20 by volume in deionized water. This provides a thin dielectric layer with a smooth surface that provides resistance to electrical breakdown.

Figure 2a,b,c shows the side (2a,b) and top (2c) views, respectively, of a static droplet of propylene glycol immersed in decane while different a.c. voltages are applied to one set of electrode fingers with

the interposed fingers maintained at earth potential. The surrounding decane liquid was contained in a cuvette with a removable lid to prevent liquid evaporation. This was sealed onto the substrate using UV-cured epoxy adhesive. The droplet was dispensed under the decane onto the electrode area of the substrate using a volume-calibrated "Gilson Pipetman" micropipette (Gilson, Middleton, WI). Electrical addressing of the device was performed with a 10 kHz sinewave voltage provided by a waveform generator connected to a PZD700A-1 amplifier (Trek, Medina, NY). The voltage was increased quasi-statically with 60 seconds between voltage increments to avoid entrainment of decane between the spread film of propylene glycol and the electrodes. Images of the immersed droplet were recorded using a standard USB video camera (DCC1645C, ThorLabs, Ely, U.K.) fitted with a 10X objective lens.

With no applied voltage (labeled 0 V) the droplet forms a spherical cap, appearing as a circular arc with a contact angle of  $125^\circ$  viewed from the sides, that is, from the  $x$  direction and from the  $y$  direction shown in Figure 2a,b, respectively, and as a circular outline viewed from the top ( $z$  direction) in Figure 2c. When the voltage is raised to 100 V (r.m.s.) the droplet adjusts position slightly in the  $x$ – $y$  plane so that its upper and lower edges in the  $x$  direction both tend to lie above gaps between electrodes rather than electrodes, its height  $h$  decreases, and its contact angle reduces to  $110^\circ$ , as shown in Figure 2a. The droplet begins to elongate in the  $y$  direction, and its outline in Figure 2c is no longer circular. At still higher voltages, 150 and 200 V, the droplet continues to flatten and reduce its height  $h$  in the  $z$  direction, while its length  $l$  in the  $y$  direction increases. At these voltages, Figure 2a,b shows that the side profile, viewed from both the  $x$  direction and the  $y$  direction, deviates from a circular arc. Interestingly, the local contact angle viewed orthogonal to the direction of spreading, that is, from the  $x$  direction, is maintained at a value that remains near to  $90^\circ$ , as shown in the contrast-enhanced magnified image of the region near the contact line in the direction of spreading at 200 V in Figure 2a. A saturation of a local contact angle has also been observed to occur at the higher voltages in electrowetting within the characteristic length-scale governing the capacitive energy of the system, that is, the thickness of the dielectric.<sup>22</sup> Here for dielectrowetting the equivalent length scale the distance between electrodes is larger.

Figure 2b,c shows that while spreading in the  $y$  direction occurs the width  $w$  in the  $x$  direction remains constant as a result of the electrode symmetry in our system. The electrodes form parallel stripes in the  $y$  direction, giving rise to a potential that is spatially varying only in one direction, the  $x$  direction. The electrostatic energy of the system is reduced when the regions of high electric field intensity between the electrodes are occupied by a material that is highly polarizable, here



**Figure 2.** Shape of a droplet of propylene glycol immersed in decane is shown viewed (a) from the  $x$  direction, (b) from the  $y$  direction, and (c) from above when different values of the a.c. sinewave voltage (r.m.s. values given) are applied to one set of electrode fingers.

the liquid with higher dielectric constant. The force to actuate liquid movement into these regions is provided via its interaction with the highly nonuniform fringing electric fields occurring in the regions close to both edges of the electrodes.<sup>23,24</sup> These forces depend on the square of the gradient in the electric field and hence direct the liquid toward the electrode gaps in the  $x$  direction but away from the lower electric field regions above the electrodes themselves. This gives rise to an effective electrostatic barrier to the liquid spreading across the regions above electrodes and acts to maintain the width of a spreading droplet to be equal to an integer number of electrode gaps.

## RESULTS AND DISCUSSION

The height  $h$  and the length  $l$  of the droplet of propylene glycol immersed in decane are plotted as a function of magnitude of the applied voltage in Figure 3. Although the values of  $h$  and  $l$

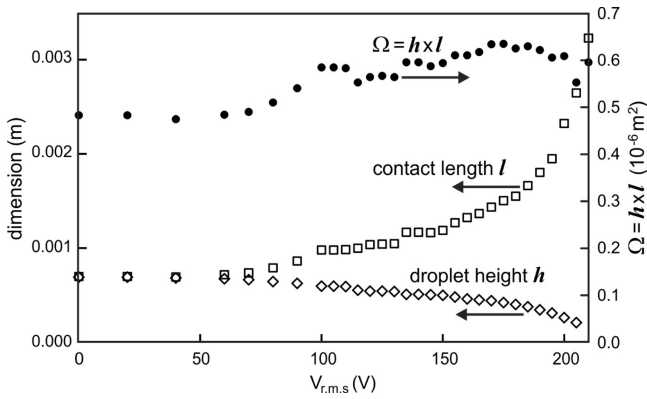


**Figure 3.** Height  $h$  (open diamonds) and the contact length  $l$  (open squares) values for the droplet of propylene glycol immersed in decane are plotted as a function of the r.m.s. value of the voltage applied to one set of electrode fingers. The values of  $h$  and  $l$  were measured from magnified images taken from the  $x$  direction, as defined in Figure 1. The product of these quantities,  $\Omega = h \times l$ , shown by the filled circles, remained relatively constant and within the range  $(0.59 \pm 0.04) \times 10^{-6} \text{ m}^2$  as the voltage was increased to 210 V. This observation, along with the flattened noncircular shapes shown during spreading at high voltages in Figure 2c, prompted us to adopt the rectangular cuboid model geometry in Figure 4l to develop a theoretical model of quasi-static dielectrophoresis driven spreading based on the balance between interfacial energies and dielectrophoretic energies.

remained similar below 50 V, the values begin to diverge at 60 V and above with the length increasing and the droplet height decreasing as the droplet spreads in the  $y$  direction and flattens. Above 100 V we observed that the product of these quantities,  $\Omega = h \cdot l$ , shown in Figure 3 by the filled circles, remained relatively constant and within the range  $(0.59 \pm 0.04) \times 10^{-6} \text{ m}^2$  as the voltage was increased to 210 V. This observation, along with the flattened noncircular shapes shown during spreading at high voltages in Figure 2c, prompted us to adopt the rectangular cuboid model geometry in Figure 4l to develop a theoretical model of quasi-static dielectrophoresis driven spreading based on the balance between interfacial energies and dielectrophoretic energies.

There are five interfaces between the cuboidal rectangular liquid droplet and the fluid in which it is immersed, and these give a contribution to the total interfacial energy,  $W_S$ , of  $[(l + 2h)w + 2hl]\gamma_{LF}$ , where  $\gamma_{LF}$  is the liquid–fluid interfacial tension. There are also contributions from the solid–liquid interface,  $lw\gamma_{SL}$ , and the solid–fluid interface,  $(l_\infty - l)w\gamma_{SF}$ , where  $\gamma_{SL}$  and  $\gamma_{SF}$  are the solid–liquid and solid–fluid interfacial tensions and  $l_\infty$  is the length of the solid surface in the  $y$  direction. Writing the cross-sectional area of the droplet as  $\Omega = hl$ , which is constant, gives the following expression for the total interfacial energy

$$W_S = w \left( \frac{\Omega}{h} + 2h \right) \gamma_{LF} + w \frac{\Omega}{h} (\gamma_{SL} - \gamma_{SF}) + 2\Omega \gamma_{LF} + w l_\infty \gamma_{SF} \quad (1)$$

This can be minimized with respect to the droplet height  $h$ , taking into account the constant width  $w$ , and hence rewritten in terms of a zero voltage equilibrium height  $h_0$ ,

$$W_S = 2wh \left( 1 + \frac{h_0^2}{h^2} \right) \gamma_{LF} + w l_\infty \gamma_{SF} + 2\Omega \gamma_{LF} \quad (2)$$

where  $h_0^2 = [1 + (\gamma_{SL} - \gamma_{SF})/\gamma_{LF}]\Omega/2$ , which can be written  $h_0^2 = [1 - \cos \theta_e]\Omega/2$  using the combination of interfacial tensions to define an equivalent Young's law contact angle for an immersed droplet.

When a dielectric fluid of permittivity  $\epsilon$  is in contact with a substrate having interdigitated electrodes to which a voltage  $V(x) = V_0 \cos(1/2\pi x/d)$  is applied, then an exponentially decaying electric field penetrates into the fluid and electrostatic energy,  $W_E$ , is stored. A 2-D solution to the Maxwell equation  $\nabla \cdot \mathbf{D} = 0$  gives  $V(x,z) = V_0 \cos(2x/\delta) \exp(-2z/\delta)$ , where  $\delta = 4d/\pi$  has been defined as a penetration depth and is determined by the periodicity of the electrodes. Integrating the electrostatic energy per unit area in the  $x$ – $y$  plane and assuming the fluid thickness is much greater than the decay length gives  $W_E = -1/2(\epsilon_0 \epsilon_F V_0^2 / \delta)$ .<sup>17</sup> In the region above the electrodes that is covered only by the immersing fluid,  $-w/2 < x < w/2$ ,  $-\infty < y < -l/2$ , and  $l/2 < y < \infty$ ; this gives the first term in the electrostatic contribution to the total energy

$$W_E = -\frac{\epsilon_0 \epsilon_F V_0^2}{2\delta} \left( l_\infty - \frac{\Omega}{h} \right) w - \frac{\epsilon_0 \epsilon_L V_0^2}{2\delta} g(h/d, \epsilon_L, \epsilon_F) \frac{\Omega}{h} w \quad (3)$$

The electrode region  $-w/2 < x < w/2$ ,  $-l/2 < y < l/2$  is covered by a liquid droplet, and there is an interface between the liquid and the immersing fluid at  $z = h$ . A model can be constructed with two fluid layers and solving Maxwell's equations with appropriate boundary conditions at each interface. The second term in eq 3 gives the analytical approximation for the electrostatic energy in this situation using the first two Fourier modes to describe the spatially periodic potential,<sup>25</sup> where the factor  $g(h/d, \epsilon_L, \epsilon_F)$  is given by

$$g(h/d, \epsilon_L, \epsilon_F) = \frac{\left( 1 - \frac{(\epsilon_L - \epsilon_F)}{(\epsilon_L + \epsilon_F)} \exp\left(-\frac{\pi h}{d}\right) \right)}{\left( 1 + \frac{(\epsilon_L - \epsilon_F)}{(\epsilon_L + \epsilon_F)} \exp\left(-\frac{\pi h}{d}\right) \right)} \quad (4)$$

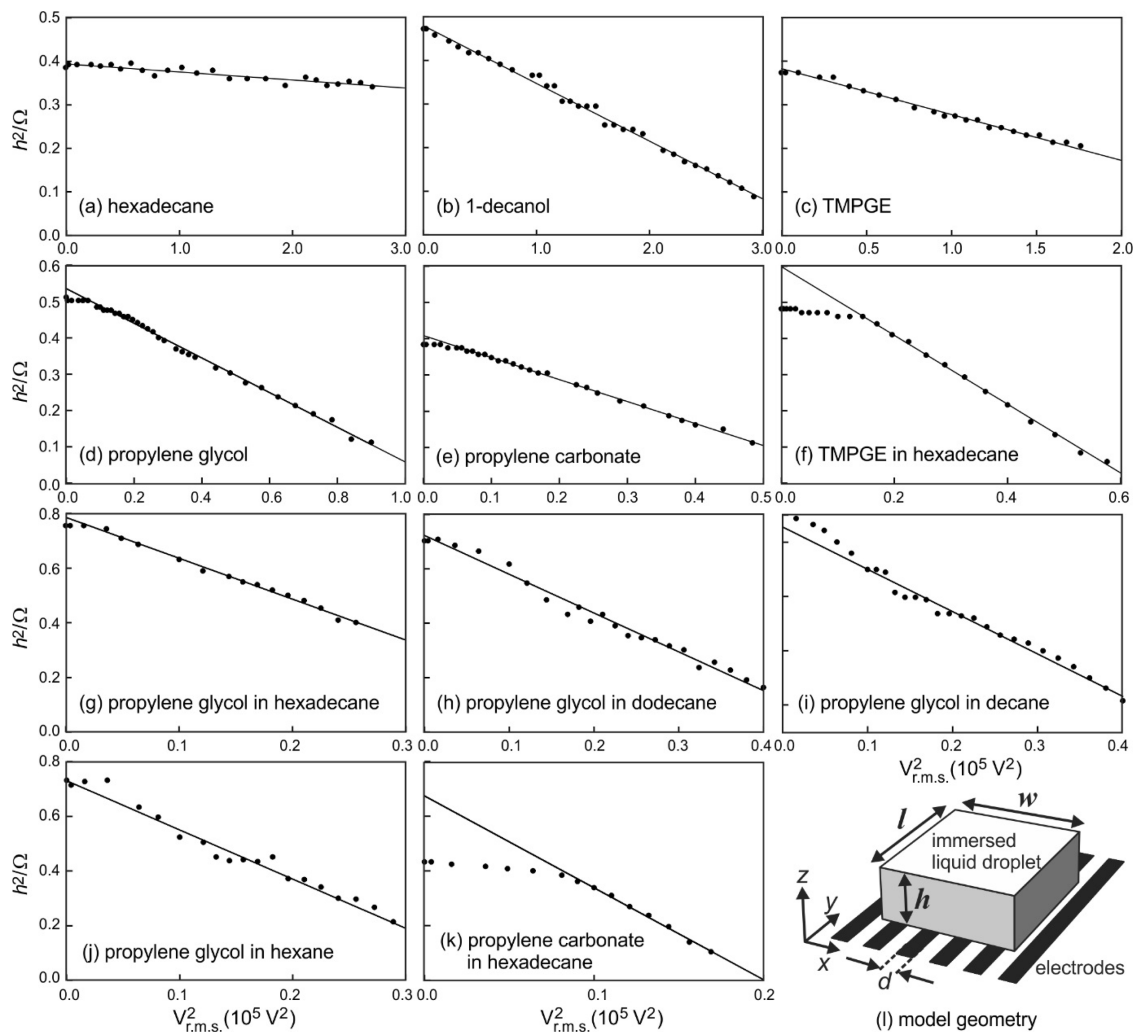
This factor can be approximated to unity provided that the spread film thickness  $h$  remains significantly larger than the electrode gap  $d$ . The expression for the total energy,  $W_T = W_S + W_E$ , is then given by

$$W_T = 2wh \left( 1 + \frac{h_0^2}{h^2} \right) \gamma_{LF} + w l_\infty \gamma_{SF} + 2\Omega \gamma_{LF} - \frac{\epsilon_0 \epsilon_F V_0^2}{2\delta} \left( l_\infty - \frac{\Omega}{h} \right) w - \frac{\epsilon_0 \epsilon_L V_0^2}{2\delta} \frac{\Omega}{h} w \quad (5)$$

The voltage-dependent height is then given by minimizing the total energy  $W_T = W_S + W_E$  with respect to the droplet height,  $h$

**Table 1.** Different Combinations of Immersed Liquid Droplet and Surrounding Liquid/Fluid That Were Used in the Experiments

droplet		immersion fluid		contact angle $\theta_e$ ( $V = 0$ )	permittivity difference $\Delta\epsilon = \epsilon_L - \epsilon_F$	interfacial tension $\gamma_{LF}$ ( $\text{mJ m}^{-2}$ )	ratio ( $\Delta\epsilon/\gamma_{LF}$ ) ( $\text{J}^{-1} \text{m}^2$ )
liquid	$\epsilon_L$	fluid	$\epsilon_F$				
hexadecane	2.05	air	1.00	$76 \pm 2$	1.05	$27.1 \pm 0.2$	$38.7 \pm 0.3$
1-decanol	7.93	air	1.00	$87 \pm 2$	6.93	$28.5 \pm 0.2$	$243 \pm 2$
TMPGE	12.7	air	1.00	$74 \pm 2$	11.7	$40.5 \pm 0.3$	$289 \pm 2$
propylene glycol	27.5	air	1.00	$91 \pm 2$	26.5	$35.5 \pm 0.3$	$747 \pm 6$
propylene carbonate	66.1	air	1.00	$75 \pm 2$	65.1	$40.9 \pm 0.3$	$1590 \pm 10$
TMPGE	12.7	hexadecane	2.05	$88 \pm 2$	10.6	$5.3 \pm 0.1$	$2000 \pm 40$
propylene glycol	27.5	hexadecane	2.05	$113 \pm 2$	25.5	$9.9 \pm 0.1$	$2580 \pm 30$
propylene glycol	27.5	dodecane	2.01	$109 \pm 2$	25.5	$9.5 \pm 0.1$	$2680 \pm 30$
propylene glycol	27.5	decane	1.99	$116 \pm 2$	25.5	$9.5 \pm 0.1$	$2680 \pm 30$
propylene glycol	27.5	hexane	1.89	$111 \pm 2$	25.6	$7.4 \pm 0.1$	$3460 \pm 50$
propylene carbonate	66.1	hexadecane	2.05	$82 \pm 2$	64.1	$10.8 \pm 0.2$	$5900 \pm 100$

**Figure 4.** (a–k) Graphs of  $h^2/\Omega$  (equivalently  $h/l$ ) plotted against the square of the r.m.s. value of the voltage for each of the different combinations of immersed liquid droplet and surrounding fluid, either air or another liquid. In the higher voltage regions where the plots are linear, a linear regression fit has been performed, shown by the solid lines. Panel l depicts the model geometry that was used in the theoretical analysis.

$$h^2(V_0) = h_0^2 - \frac{\epsilon_0 \Delta\epsilon V_0^2 \Omega}{4\delta\gamma_{LF}} \quad (6)$$

where  $\Delta\epsilon = (\epsilon_L - \epsilon_F)$  is the contrast in relative permittivity between the fluid and the droplet. Equation 6 predicts that on a given substrate a stripe droplet spreading due to dielectrowet-

ting as a rectangular cuboid of constant width will reduce the square of its thickness in proportion to the square of the applied voltage with a gradient proportional to  $\Delta\epsilon/\gamma_{LF}$ .

Previous reports of the use of dielectric forces for optofluidics have tended to employ circular electrode geometries to promote axially symmetric immersed droplet actuation.<sup>15,16</sup> In

the form used they rise to nonuniform dielectric forces that strongly vary with radius, and so these geometries are not so readily accessible to such an analytical theoretical approach to describing the dependence of the wetting on the voltage.

To test the effectiveness of eq 6 further, we performed a systematic series of experiments using droplets of hexadecane, 1-decanol, trimethylolpropane triglycidyl ether (TMPGE), propylene glycol, and propylene carbonate with relative permittivity  $\epsilon_L = 2.05, 7.93, 12.7, 27.5,$  and  $66.1,$  respectively, in air, hexadecane, dodecane, decane, hexane, and hexadecane with  $\epsilon_F = 1.0, 2.05, 2.01, 1.99, 1.89,$  and  $2.05,$  respectively (Table 1). We used pendant drop measurements (drop shape analysis, A. Krüss Optronic, Hamburg, Germany) to obtain the liquid–fluid interfacial tensions, and these ranged from  $(5.3 \pm 0.1) \text{ mJ m}^{-2}$  to  $(40.9 \pm 0.3) \text{ mJ m}^{-2}$ . The equilibrium contact angles at zero voltage,  $\theta_e (V = 0)$ , for each of the immersed liquid droplets that were studied in the experiments are also given in Table 1. The liquid–fluid combinations used spanned a range of more than two orders of magnitude of  $\Delta\epsilon/\gamma_{LF}$  from  $(38.7 \pm 0.3)$  to  $(5900 \pm 100) \text{ J}^{-1} \text{ m}^2$ . Figure 4a–k shows the measured value of  $h^2/\Omega$  plotted against the square of the r.m.s. value of the voltage, which is half the peak voltage  $V_o$ , used in eq 6, because our AC voltage is applied to every other electrode with the interposed electrodes at earth potential. In several cases there is a clear hysteresis, an initial centering of the droplet on the set of electrodes at the lower voltages, before spreading in a rectangular cuboid shape occurs, and the linear relationship between  $h^2/\Omega$  and  $V_{\text{rms}}^2$  is then obtained only at the higher voltages. Interestingly, for some of the liquid/fluid combinations in Figure 3, especially those liquid/fluid combinations with smaller values of the parameter  $\Delta\epsilon/\gamma_{LF}$ , the data do appear to also fall onto the same linear fit for the whole range of the voltages shown.

For the range of liquid–air and liquid–liquid combinations given in Table 1, the factor  $g(h/d, \epsilon_L, \epsilon_F)$  defined in eq 4 only drops to below 0.99 when  $h < 1.68d$  for  $\Delta\epsilon = 65.1$  and when  $h < 1.35d$  for  $\Delta\epsilon = 1.05$ . This is not significant in the voltage range where the spread film thickness  $h$  remains significantly larger than the electrode gap  $d$ , as is the case where the linear relationships apply in Figure 4.

According to eq 6 the gradient  $m$  of each plot should be directly proportional to the ratio of the materials parameters,  $\Delta\epsilon/\gamma_{LF}$ , where the coefficient of proportionality (given how the voltage is applied in the experiment) is predicted to be  $(\epsilon_o/16\delta) = 5.43 \times 10^{-9} \text{ J V}^{-2} \text{ m}^{-2}$ . This is in excellent agreement with the data summarized in Figure 5, which has an experimentally determined value of  $(5.6 \pm 0.1) \times 10^{-9} \text{ J V}^{-2} \text{ m}^{-2}$ .

Equation 6 implies that there would be an extrapolated voltage at which the film thickness would be zero. The mathematical form of eq 6 results from making the assumption that  $g(h/d, \epsilon_L, \epsilon_F) = 1$ . In reality, however,  $g(h/d, \epsilon_L, \epsilon_F)$  deviates from unity as the film thickness decreases and the height of the liquid–fluid interface above the substrate comes down to within the penetration length  $\delta$ . In this higher voltage regime we would expect a wrinkle deformation to develop at the liquid–fluid interface with amplitude that increases as the voltage is further increased. We observed this wrinkling effect at relatively lower voltages in previous work<sup>18</sup> on dielectrophoresis-induced spreading because we started from droplets with equilibrium contact angles  $\theta_e (V = 0)$  that were significantly lower than those used in the current work.

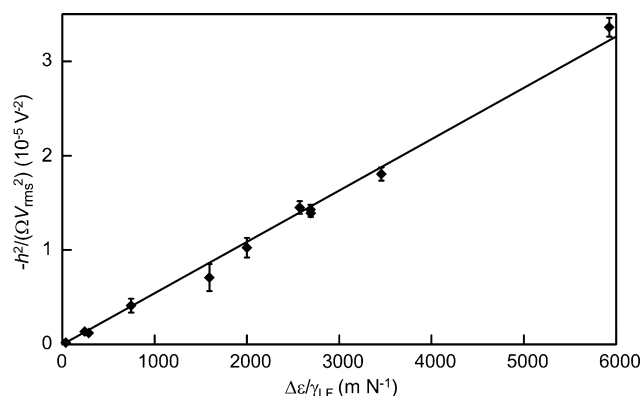


**Figure 5.** Gradients of the graphs in Figure 3a–k (i.e.,  $h^2/\Omega = h/l$  versus the square of the r.m.s. voltage value) are plotted against the ratio  $(\Delta\epsilon/\gamma_{LF})$ . Each data point, shown by the filled diamonds in the Figure, is derived from data from one of the 11 different combinations of immersed liquid droplet and surrounding liquid/fluid used in the study.  $\Delta\epsilon = \epsilon_F - \epsilon_L$  is the difference between the permittivity of the immersed liquid and the permittivity of the surrounding liquid/fluid, and  $\gamma_{LF}$  is the interfacial surface tension for each combination, as shown in Table 1

## SUMMARY AND CONCLUSIONS

Our measurements show that it is possible to quantitatively describe the liquid-dielectrophoresis-induced spreading of a dielectric liquid droplet immersed in a second fluid. The excellent agreement between the data and theory suggests the value of  $\Delta\epsilon/\gamma_{LF}$  for a liquid with unknown properties for either the permittivity of one of the fluids or of the liquid–fluid interfacial tension could be determined in a simple manner. The principles of liquid-in-fluid dielectrowetting should be applicable to lossy dielectric liquids at higher frequencies, such as water.<sup>13</sup> Finally, the ability to perform dielectrowetting in liquid-in-liquid systems with the potential for optical contrast provides the opportunity to develop applications where density matching to provide neutral buoyancy may be important, such as a shock-resistant programmable diffraction grating.

## AUTHOR INFORMATION

### Corresponding Author

\*E-mail: carl.brown@ntu.ac.uk

### Notes

The authors declare no competing financial interest.

## ACKNOWLEDGMENTS

We gratefully acknowledge the financial support of the UK EPSRC (Grants EP/K014803/1 and EP/E063489/1).

## REFERENCES

- (1) Adamson, A. W.; Gast, A. P. *Physical Chemistry of Surfaces*, 6th ed; Wiley: New York, 1997.
- (2) Ivanova, N. A.; Starov, V. M. Wetting of low free energy surfaces by aqueous surfactant solutions. *Curr. Opin. Colloid Interface Sci.* **2011**, *16* (4), 285–291.
- (3) Quéré, D. Wetting and roughness. *Annu. Rev. Mater. Res.* **2008**, *38*, 71–99.
- (4) Shirtcliffe, N. J.; McHale, G.; Atherton, S.; Newton, M. I. An introduction to superhydrophobicity. *Adv. Colloid Interface Sci.* **2010**, *161*, 124–138.
- (5) Wong, T.-S.; Kang, S. H.; Tang, S. K. Y.; Smythe, E. J.; Hatton, B. D.; Grinthal, A.; Aizenberg, J. Bioinspired self-repairing slippery

surfaces with pressure-stable omniphobicity. *Nature* **2011**, *477* (7365), 443–447.

(6) Berge, B. Electrocapillarity and Wetting of Insulator Films by water. *C. R. Acad. Sci., Ser. II* **1993**, *317* (2), 157–163.

(7) Mugele, F.; Baret, J.-C. Electrowetting: From basics to applications. *J. Phys.: Condens. Matter* **2005**, *17* (28), R705–R774.

(8) Berge, B.; Peseux, J. Variable focal lens controlled by an external voltage: An application of electrowetting. *Eur. Phys. J. E* **2000**, *3* (2), 159–163.

(9) Hayes, R. A.; Feenstra, B. J. Video-speed electronic paper based on electrowetting. *Nature* **2003**, *425* (6956), 383–385.

(10) Fair, R. B. Digital microfluidics: is a true lab-on-a-chip possible? *Microfluid. Nanofluid.* **2007**, *3* (3), 245–281.

(11) Pollack, M. G.; Pamula, V. K.; Srinivasan, V.; Eckhardt, A. E. Applications of electrowetting-based digital microfluidics in clinical diagnostics. *Expert Rev. Mol. Diagn.* **2011**, *11* (4), 393–407.

(12) Chevalliot, S.; Kuiper, S.; Heikenfeld, J.; Adhes, J. Experimental Validation of the Invariance of Electrowetting Contact Angle Saturation. *Sci. Technol.* **2012**, *26* (12), 1909–1930.

(13) Jones, T. B.; Gunji, M.; Washizu, M.; Feldman, M. J. Dielectrophoretic liquid actuation and nanodroplet formation. *J. Appl. Phys.* **2001**, *89* (2), 1441–1448.

(14) Cheng, C.-C.; Chang, C. A.; Yeh, J. A. Variable focus dielectric liquid droplet lens. *Opt. Express* **2006**, *14* (9), 4101–4106.

(15) Yang, C.-C.; Yang, L.; Tsai, C. G.; Jou, P. H.; Yeh, J. A. Fully developed contact angle change of a droplet in liquid actuated by dielectric force. *Appl. Phys. Lett.* **2012**, *101* (18), 182903.

(16) Xu, S.; Ren, H.; Wu, S.-T. Dielectrophoretically tunable optofluidic devices. *J. Phys. D: Appl. Phys.* **2013**, *46* (48), 483001.

(17) McHale, G.; Brown, C. V.; Newton, M. I.; Wells, G. G.; Sampara, N. Dielectrowetting Driven Spreading of Droplets. *Phys. Rev. Lett.* **2011**, *107* (18), 186101.

(18) Brown, C. V.; Wells, G. G.; Newton, M. I.; McHale, G. Voltage-programmable liquid optical interface. *Nat. Photonics* **2009**, *3* (7), 403–405.

(19) Zhao, R.; Cumby, B.; Russell, A.; Heikenfeld, J. Large area and low power dielectrowetting optical shutter with local deterministic fluid film breakup. *Appl. Phys. Lett.* **2013**, *103* (22), 223510.

(20) Russell, A.; Kreit, E.; Heikenfeld, J. Scaling Dielectrowetting Optical Shutters to Higher Resolution: Microfluidic and Optical Implications. *Langmuir* **2014**, *30* (18), 5357–5362.

(21) McHale, G.; Brown, C. V.; Sampara, N. Voltage-induced spreading and superspreading of liquids. *Nat. Commun.* **2013**, *4*, 1605.

(22) Buehrle, J.; Mugele, F. Equilibrium drop surface profiles in electric fields. *J. Phys.: Condens. Matter* **2007**, *19* (37), 375112.

(23) Pohl, H. A. Dielectrophoresis: The Behaviour of Neutral Matter in Non-Uniform Electric Fields. In *Cambridge Monographs on Physics*; Cambridge University Press: Cambridge, U.K., 1978.

(24) Lorrain, P.; Corson, D. R. *Electromagnetic Fields and Waves*, 2nd ed.; Freeman: San Francisco, CA, 1970.

(25) Brown, C. V.; McHale, G.; Mottram, N. J. Analysis of a static undulation on the surface of a thin dielectric liquid layer formed by dielectrophoresis forces. *J. Appl. Phys.* **2011**, *110* (2), 024107.